

Defect engineering of the electronic transport through cuprous oxide interlayers

Mohamed M. Fadlallah^{1,2,3}, Ulrich Eckern¹, and Udo Schwingenschlög^{1*}

¹*Institut für Physik, Universität Augsburg, 86135 Augsburg, Germany*

²*Centre for Fundamental Physics, Zewail City of Science and Technology, Giza, Egypt*

³*Physics Department, Faculty of Science, Benha University, Benha, Egypt*

⁴*KAUST, PSE Division, Thuwal 23955-6900, Kingdom of Saudi Arabia*

Abstract

The electronic transport through Au-(Cu₂O)_n-Au junctions is investigated using first-principles calculations and the nonequilibrium Green's function method. The effect of varying the thickness (i.e., n) is studied as well as that of point defects and anion substitution. For all Cu₂O thicknesses the conductance is more enhanced by bulk-like (in contrast to near-interface) defects, with the exception of O vacancies and Cl substitutional defects. A similar transmission behavior results from Cu deficiency and N substitution, as well as from Cl substitution and N interstitials for thick Cu₂O junctions. In agreement with recent experimental observations, it is found that N and Cl doping enhances the conductance. A Frenkel defect, i.e., a superposition of an O interstitial and O substitutional defect, leads to a remarkably high conductance. From the analysis of the defect formation energies, Cu vacancies are found to be particularly stable, in agreement with earlier experimental and theoretical work.

PACS numbers: 73.20.-r, 73.40.Rw

Keywords: Density functional theory, oxide, point defect, doping, transport

* udo.schwingenschlogl@kaust.edu.sa, +966(0)544700080

Low production costs and the right band gap are key factors for applications of p-type semiconductors. Cuprous oxide (Cu_2O) fulfils both criteria, making the material interesting for optoelectronic devices [1], coatings [2], sensors [3], etc. It has a simple cubic structure with lattice constant $a = 4.27 \text{ \AA}$ and a direct band gap at the center of the Brillouin zone, experimentally given by 2.17 eV; see Ref. 4 for a recent review. From the theoretical point of view, Hartree-Fock and semi-empirical extended Hückel methods have been used for describing the electronic structure, resulting in massive overestimations of the band gap [5, 6]. On the other hand, density functional theory underestimates the gap, giving 0.5 to 0.7 eV within the local density approximation (LDA) [6, 7], 0.99 eV using the LDA+U approach [7], and 1.08 eV using the self-interaction correction method [8]. The Heyd-Scuseria-Ernzerhof (HSE06) hybrid functional gives a band gap of 2.02 eV, close to the experimental value [7]. All the above mentioned first-principles approaches find the valence band maximum to be dominated by Cu $3d$ states, and the conduction band minimum by Cu $4s$ states, though hybridization is important for the material properties [5, 6, 9].

Vacancies and interstitial defects in Cu_2O have been studied experimentally for many years, for example, O and Cu vacancies as well as Cu interstitials in Refs. 10–15. The effect of doping with nonmetallic anions at the O site has been investigated for Cl [16] and N [17, 18]; when doping with Si, Cu vacancy sites are preferably occupied [19, 20]. Cation doping at the Cu site has been reported for various metals, including Be [21], Mn [22], Co [23], Ni [24, 25], Ag [26], and Cd [27, 28]. As concerns the theoretical methods, the generalized gradient approximation (GGA) has been employed to investigate the effects of O and Cu vacancies, anti-sites, and interstitials [9, 29]. The GGA+U approach has been used to study the effects of Mn, Fe, Co, and Ni substitutional doping on the electronic and magnetic properties, indicating the possibility of long-range ferromagnetism when O and Cu vacancies are introduced [30]. GGA calculations also have been reported for doping with the transition metals Ag, Ni, and Zn [31]. Ag substitutional doping turns out to reduce only the band gap, whereas Zn doping leads to n-type conduction.

Since the performance of a device usually is dominated by interface properties [32, 33], Cu/ Cu_2O and Au/ Cu_2O interfaces have been addressed in Refs. 34 and 32, respectively. In particular, $\text{In}_2\text{S}_3/\text{Cu}_2\text{O}$ [35] and $\text{ZnO}/\text{Cu}_2\text{O}$ [36] interfaces have been found to be promising for photovoltaic applications. From the experimental point of view, the electrical resistivities of a Cu_2O thin film between two gold leads using SiO_2/Si substrates [37], and of a sulfur-

treated n-type Cu_2O thin film with Ag, Cu, Au, or Ni front contacts have been measured [38]. However, very little is known about the *theoretical understanding* of electronic transport properties of heterojunctions involving Cu_2O .

In order to provide insight into this question, we study in the following prototypical $\text{Au}-(\text{Cu}_2\text{O})_n\text{-Au}$ junctions including different kinds of defects such as vacancies (O or Cu), substitutional, interstitial (N or Cl) and Frenkel defects at different positions in the structures. We carefully optimize the atomic positions, in order to obtain physically relevant results. Note that in the main text our focus is on the optimized structures; but in most figures we include also the results for the unrelaxed structures for comparison, including some brief comments in order to highlight relevant changes due to relaxation. As is apparent from the results, the optimization of the structures strongly affects the electronic structure and transport properties such as the transmission coefficient and the conductance. Generally bulk defects are more effective for enhancing transport than near-interface defects. In order to increase the conductance we suggest that interstitial defects are more suitable than substitutional ones.

We note from the start that formally, one defect for the $n = 4$ junction corresponds to a defect concentration of 3.8 %. We also wish to emphasize that the comparison of our model results with experimental data can only be qualitative, since the latter strongly depend on the method of preparation, as well as the concrete substrate—which we are, at least at present, not able to incorporate in a quantitative way.

RESULTS

Using SIESTA [39] as electronic structure package, the transport properties are calculated by the SMEAGOL [40–42] code, which employs the nonequilibrium Green’s functions method. Periodic boundary conditions are applied perpendicular to the [100] transport direction. The Perdew-Burke-Ernzerhof version [43] of the GGA is utilized for the exchange-correlation potential. Moreover, the energy cutoff is set to 250 Ry, and Monkhorst-Pack k-meshes of $15 \times 15 \times 25$ points for the leads and $15 \times 15 \times 1$ points for the transport calculations are used. Norm-conserving pseudopotentials are employed (fully nonlocal Kleinman-Bylander type [44] with double-zeta basis set). The pseudopotentials for the Cu, O and Cl atoms include nonlinear core corrections in the exchange correlation potential [45]. The

basis set superposition error is corrected using the counterpoise procedure [46].

A lattice strain of 4 % is introduced by assuming an epitaxial interface, and therefore setting the Cu_2O lattice constant to the Au value of 4.09 Å. All structural optimizations (relaxations) are based on the conjugate gradient method, converging the net force on each atom down to 0.04 eV/Å. The leads are modeled by two atomic layers of face centered cubic [001] Au; in addition, four Au layers on each side of the $(\text{Cu}_2\text{O})_n$ layer are included in the scattering region. We study Au- $(\text{Cu}_2\text{O})_n$ -Au junctions comprising $n = 1$ to 4 Cu_2O unit cells, which corresponds to 3 to 9 atomic layers of Cu_2O .

Comparison to previously published theoretical results on bulk Cu_2O and Au shows good agreement with our calculations for the bulk materials [7]. The well-known fact that GGA underestimates the *bulk band gap* indeed is an issue of debate, but we take here the point of view that, since the band dispersions are qualitatively correctly described by first-principles calculations, a correct description of *transport through small heterostructures* can be expected, in particular, concerning the defect and doping dependence.

The pristine and defective heterojunctions under study are displayed in Fig. 1. We consider, in particular, defects at or near the interface (near-interface), as well as in the bulk (bulk-like). Concerning O, we study O vacancies near-interface, Fig. 1(c), and bulk-like, Fig. 1(d), and O interstitials near-interface, Fig. 1(e), and in the bulk (not presented in Fig. 1). Furthermore, Cu vacancies at the interface, Fig. 1(f), and in the bulk, Fig. 1(g), are addressed. For Frenkel defects, where an O atom is removed from a certain layer and inserted into another one, there are two possibilities, near-interface, Fig. 1(h), and bulk-like, Fig. 1(i). Finally, N and Cl substitutional and interstitial defects are also considered at different positions in the structure.

Due to the contact between Au and Cu_2O , the optimization changes the positions of the atoms at the interface and in the bulk of the Cu_2O interlayer; for pristine junctions, e.g., the Au-Cu distance at the interface is reduced by about 4 % due to relaxation. Defects, even those that are two layers away from the interface, alter the atomic positions further: in fact the additional shift of Cu towards Au at the interface is maximal for the cases (e), (g), and (h) in Fig. 1 (another 6 %).

The defect formation energies give an indication which defects are more likely to be of experimental relevance than others; it is defined as the energy of the defective structure,

minus the energy of the respective “constituents”:

$$E_{\text{formation}}^{\text{defective}} = E_{\text{total}}^{\text{defective}} - E_{\text{total}}^0, \quad (1)$$

where the subscript “total” refers to the respective total energies. For example, for an X vacancy, E_{total}^0 is given by the total energy of the pristine structure, from which the energy of a single X atom is subtracted:

$$E_{\text{total}}^0 = E_{\text{total}}^{\text{pristine}} - E_X \quad (\text{vacancy}). \quad (2)$$

In particular, we determine E_{Cu} from the Cu bulk energy, while we assume E_{O} to be half the molecular energy. For a substitutional defect, where the atom X is replaced by the atom Y, we have

$$E_{\text{total}}^0 = E_{\text{total}}^{\text{pristine}} - E_X + E_Y \quad (\text{substitution}). \quad (3)$$

The argumentation for interstitial and Frenkel defects proceeds similarly.

The formation energies—as well as the respective conductances, to be discussed below—are given in Table I. It is apparent that O interstitials are by far the most stable defects among the ones considered, followed by Cu vacancy bulk-like, N interstitial bulk-like, and bulk-like Frenkel defects. Generally bulk-like defects are more favorable than interfacial ones except for O vacancies, N interstitial and Cl substitutional defects. The stability of structures with Cu vacancies observed here was noticed in previous theoretical studies [47–49], and was also seen experimentally [50–53].

A. Pristine junction

The projected density of states (PDOS) of the interfacial atoms for the pristine Au–Cu₂O–Au heterojunction is shown in Fig. 2 (left). Broad Cu 3*d* and Au 5*d* states are apparent, as well as signs of Cu–Au hybridization, particularly at –2 eV. Figure 2 (right) refers to the bulk-like O and Cu atoms in the center of the Cu₂O region for $n = 1$ and $n = 4$. The enhanced Cu–O hybridization around –1 eV is characteristic for the $n = 1$ case. Down to about –5 eV we observe the expected dominance of Cu 3*d* states, the DOS structure being broader for $n = 1$.

The transmission coefficients and thickness (n) dependencies are shown in Fig. 3. For the optimized structure (right), $T(E)$ reflects the shape of the DOS below the Fermi energy,

E_F , compare Fig. 2: most notable are the peak near -3 eV (due to the localized Cu levels), as well as the almost constant DOS above E_F (due to the extended Cu states). We expect that the transmission at E_F is dominated by Cu states, since Cu is located next to Au in the junctions studied. The corresponding conductance, $G = G_0 T(E_F)$, is of the order of $0.15 G_0$ (for $n = 1$), where $G_0 = 2e^2/h$ denotes the conductance quantum (the factor 2 is due to the spin). Increasing n to 4, the conductance drops to $0.014 G_0$.

Above E_F , $T(E)$ increases roughly linearly with energy due to the delocalized Cu 4s states. The transmission decreases with increasing thickness n . A transport gap of approximately 0.6 eV appears for the relaxed structure when increasing n to 4. For any thickness studied the heterojunction behaves as an n-type conductor. In the following, we omit the results for $n = 3$ since they are similar to those for $n = 4$.

B. O and Cu defects

First we discuss the role of O and Cu vacancies and O interstitial defects, cf. Fig. 1, (c)–(g), as well as of Frenkel defects, which consist of an O vacancy and an O interstitial, cf. Fig. 1, (h) and (i).

Figure 4 shows $T(E)$ for O vacancies (top part of the figure) and O interstitial defects (bottom part of the figure). In the following, we concentrate our discussion on the optimized structures (right). A major change of the transmission, compared to the pristine junction, is observable for both cases for $n = 1$, namely a shift of weight from the peak around -3 eV towards E_F , and an enhancement below -5 eV. However, $T(E)$ is more evenly distributed for an interstitial defect. In addition, $T(E)$ is enhanced at the Fermi energy by vacancies due to contributions from Au and Cu states, as is apparent from the respective PDOS (not shown here). The conductance is $0.82 G_0$, and thus considerably larger than in the pristine case.

For the thicker Cu_2O layer, $n = 4$, we consider O vacancies at the interface and in the center of the Cu_2O region, see Fig. 1, (c) and (d). The exact position of the vacancy plays only a minor role for $T(E)$. As compared to the pristine junction, the transport gap at E_F has closed, but the conductance is rather small, about $0.063 G_0$ and $0.035 G_0$ for the near-interface and bulk-like vacancy, respectively.

An O interstitial atom in a thin ($n = 1$) Cu_2O interlayer results in a significant $T(E)$

down to -8 eV, see Fig. 4 (rightmost). Furthermore, the minimum of $T(E)$ around E_F is completely washed out, resulting in enhanced conductances of $0.41 G_0$ (near-interface) and $0.62 G_0$ (bulk-like). However, the enhancement is slightly less than what is observed for O vacancies. For the thick ($n = 4$) Cu_2O layer the effect of an interstitial O atom strongly depends on its position: the conductance is considerably higher for the bulk-like than for the near-interface interstitial ($0.11 G_0$ vs. $0.02 G_0$). This fact can be related to a strong contribution of p orbitals, which lead to a clearly visible peak in the O (bulk-like) PDOS at E_F , even larger than the Cu (bulk-like) PDOS. For a near-interface interstitial, on the other hand, this peak is located near -1 eV. Overall $T(E)$ behaves similar to the pristine junction.

In Fig. 5 we show the transmission coefficients for Cu vacancies; we focus again the discussion on the optimized structures (right). As compared to the pristine junction, vacancies enhance $T(E)$ below -5 eV for $n = 1$. For an interfacial Cu vacancy the change in $T(E)$ below E_F can be related to the sensitivity of the d bands to disorder, and the Au($5d$)–Cu($3d$) orbital interaction at the interface [54]. The conductance is reduced (compared to the pristine junction) to $0.12 G_0$ ($n = 1$). For a bulk-like Cu vacancy an enhanced $T(E)$ is visible between -5 and -4 eV due to contributions from Cu 3d bulk states, and the conductance is given by $0.52 G_0$. An increase of the conductance due to Cu vacancies is in agreement with previous work on thin films [15]. Independent of its position, a Cu vacancy shifts the minimum of $T(E)$ around E_F to higher energy.

On the other hand, for a thick ($n = 4$) Cu_2O layer, the gross shape of $T(E)$ for Cu vacancies is very similar to the case of O vacancies. The conductance, however, is higher for the bulk-like than for the interfacial Cu vacancy ($0.032 G_0$ vs. $0.026 G_0$). Note that the conduction type can be modified by Cu vacancies.

Turning to Fig. 6, we observe that a Frenkel defect modifies $T(E)$ substantially for $n = 1$, leading to a very high conductance of $0.92 G_0$. For $n = 4$ we consider the two Frenkel defect configurations shown in Fig. 1, (h) and (i). We find no significant difference in $T(E)$, and obtain essentially the same conductance (0.070 vs. $0.075 G_0$) for both of them. Roughly speaking, $T(E)$ can be considered a combination of the effects of an O vacancy and an O interstitial.

C. N and Cl doping

The effect of N substitutional and interstitial doping is addressed in Fig. 7. Clearly the onset of $T(E)$ is related to the energetic positions of the N relative to the Cu states, and the high $T(E)$ around -6.5 eV is due to a strong overlap between them. Minima in $T(E)$, for example near -4 eV, coincide with minima in the Cu PDOS (not shown here). The shift of the minimum of $T(E)$ around E_F to higher energy is similar to the effect of a Cu vacancy. Conductance values of $0.40 G_0$, $0.74 G_0$, and $0.99 G_0$ are obtained for N substitution, near-interface N interstitial, and bulk-like N interstitial, respectively ($n = 1$). Substitution creates an excess hole, while an interstitial defect creates excess electrons. This explains why the conductance is higher for the interstitial than for the substitutional case. For bulk-like N interstitial there are more transmission channels than for the near-interface N interstitial at E_F .

Figure 7 also deals with N doping at different positions for $n = 4$. Comparing substitutional and interstitial doping, the overall energy dependence is quite similar (and similar to the pristine junction), except for subtle differences near E_F . As compared to the pristine junction, the transport gap is slightly reduced, and the conductance thus a little enhanced, similarly for bulk-like and near-interface substitution, to about $0.015 G_0$. Turning to N interstitial defects ($n = 4$), Fig. 7 shows that the bulk-like position of the defect results in a slightly higher conductance than the near-interface position, $0.061 G_0$ vs. $0.031 G_0$.

Figure 8 addresses Cl doping. For $n = 1$ substitutional doping, we find close similarities to the pristine junction though the minimum near E_F has shifted to lower energy, which is opposite to what is found for N doping. The conductance of about $0.34 G_0$ accordingly is higher than in the pristine junction, but lower than in the case of N doping. The shift of the minimum of $T(E)$ to lower energy appears also for the Cl interstitial defect. A bulk-like Cl interstitial defect leads to a higher conductance ($0.56 G_0$) than a near-interface Cl interstitial defect ($0.32 G_0$).

Interestingly, see Fig. 8, for $n = 4$ we find again a shift of the minimum of $T(E)$ near E_F to higher energy (compared to the pristine case) for the bulk-like Cl substitutional defect. The conductances are given by $0.065 G_0$ and $0.043 G_0$ for near-interface and bulk-like substitution, respectively, which is considerably higher than for N substitution. In contrast to the other cases considered, the Cl bulk-like substitution has a *lower* conductance

than the near-interface one. The overall results for Cl interstitials are similar to those for N interstitial defects, but with slightly smaller conductances ($0.022 G_0$ for the near-interface, and $0.033 G_0$ for the bulk-like case). The calculated conductances for $n = 4$ are summarized in Table I.

DISCUSSION

Based on the density functional theory and the nonequilibrium Green's function approach, a comprehensive study of the electronic structure and transport properties of Au-(Cu₂O)_n-Au heterojunctions of different thickness, with different point defects, and with different kinds of anion doping of Cu₂O has been carried out. As to be expected, the transmission decreases with increasing n . Compared to the pristine junction, we find for thin interlayers, $n = 1$, for O vacancies and for interstitial O, N, and Cl defects a drastic change of $T(E)$ around the Fermi energy. Bulk-like defects are found to enhance the transport more effectively than near-interface defects—which appears reasonable since the system has a better chance to adjust to a bulk-like compared to a near-interface disturbance, thereby reducing scattering. Accordingly, we also find that for all cases considered the formation energy is lower for bulk-like than for interface or near-interface disturbances.

Experimentally it has been found that N and Cl doping enhances the conductance [16, 17], and that interstitial N defects are more effective than N substitution [18]. While this agrees with our findings, further work is needed to establish the connection between the present model studies and the actual experimental situation, where, in particular, the film thicknesses are much larger than the ones in our model. Note that for Cl we observe the opposite trend: interstitial defects are less effective than substitution. In conclusion, our investigation provides indications on how to improve the electrical and photovoltaic properties of Cu₂O contacted by two gold leads, namely by appropriate, preferably bulk-like defect engineering. Of course, it must be kept in mind that the detailed experimental conditions may not always be properly reflected by the idealized theoretical modelling.

ACKNOWLEDGMENTS

We acknowledge financial support by the Deutsche Forschungsgemeinschaft (through

TRR 80). Research reported in this publication was supported by the King Abdullah University of Science and Technology (KAUST).

AUTHOR CONTRIBUTIONS

M.M.F. performed the calculations. All authors contributed to the analysis of the results and the writing of the manuscript.

ADDITIONAL INFORMATION

The authors declare no competing financial interests.

TABLE I. Formation energies $\Delta E \equiv E_{\text{formation}}^{\text{defective}}$ (in units of eV), and conductances G (in units of $10^{-2}G_0$, $G_0 = 2e^2/h$, for $n = 4$). For comparison, the conductance of the pristine junction is given by $1.4 \times 10^{-2}G_0$ ($n = 4$): thus the conductance of the defective junctions can be up to a factor of about 8 (for O interstitials, bulk-like) larger than for the “clean” case.

	ΔE	G	O	ΔE	G	N	ΔE	G	Cl	ΔE	G
O vacancy, near interf.	0.3	5.8	interst., near interf.	-0.2	2.0	interst., near interf.	0.1	3.1	interst., near interf.	-0.1	2.2
O vacancy, bulk-like	0.4	3.2	interst., bulk-like	-1.7	11	interst., bulk-like	-1.1	6.1	interst., bulk-like	-0.2	3.3
Cu vacancy, at interf.	-0.3	2.6	Frenkel, near interf.	0.8	7.0	subst., near interf.	2.0	1.5	subst., near interf.	1.1	6.5
Cu vacancy, bulk-like	-1.6	3.2	Frenkel, bulk-like	-0.8	7.5	subst., bulk-like	1.0	1.4	subst., bulk-like	1.9	4.3

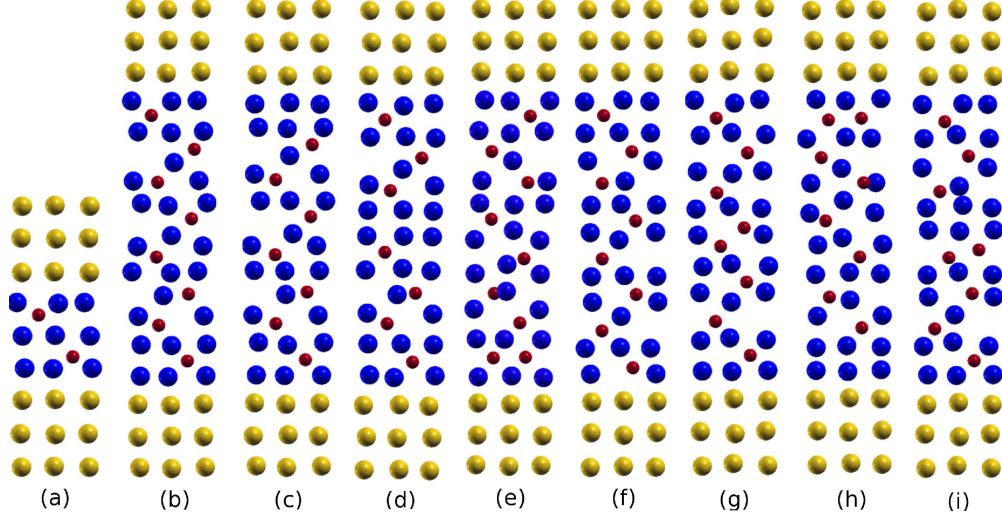


FIG. 1. (Color online) Structurally optimized Au-(Cu₂O)_n-Au heterojunctions for $n = 1$ (pristine, (a)) and $n = 4$ (pristine, (b)); O vacancy close to the interface, (c); O vacancy in the center, (d); interstitial O atom close to the interface, (e); Cu vacancy close to the interface, (f); Cu vacancy in the center, (g); two configurations of Frenkel defects, (h), “near-interface”, and (i), “bulk-like”. Yellow, blue, and red spheres represent Au, Cu, and O atoms, respectively.

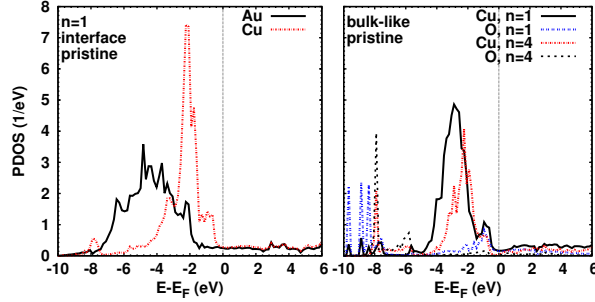


FIG. 2. (Color online) Projected DOS of atoms at the interface (left) and in the center of the Cu₂O region for $n = 1$ and $n = 4$ (right), after structural relaxation

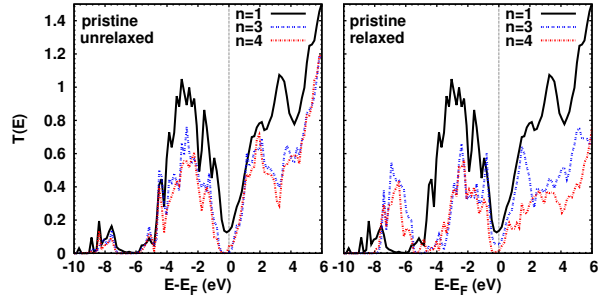


FIG. 3. (Color online) Transmission coefficient for unrelaxed (left) and relaxed (right) heterojunctions. While for the unrelaxed system there is hardly any difference between $n = 3$ and 4, the transport gap appears for the relaxed structure only for $n = 4$. A pronounced transmission around -7 eV appears for the relaxed structure for $n = 3$ and 4, due to significant contributions from Au–Cu interface states (which are absent in the case of $n = 1$). For energies far above E_F , the transmission is somewhat reduced upon relaxation for $n = 3$ and 4. On the other hand, hardly any change due to the optimization process is observed for $n = 1$.

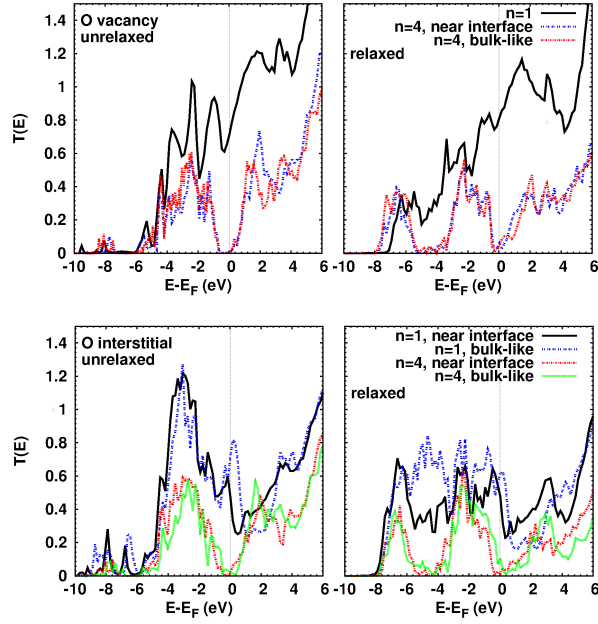


FIG. 4. (Color online) Transmission coefficient for O vacancies (top) and interstitials (bottom), before (left) and after (right) structural optimization; compare Fig. 1, (c), (d), and (e). The pronounced transport gap found for O vacancies ($n = 4$) before relaxation is filled due to structural optimization. On the other hand, there is hardly any relaxation effect for vacancies for $n = 1$, while it appears largest for O interstitial doping. The transmission at E_F generally is higher when the atomic positions are optimized, and that bulk-like defects lead to a higher transmission than near-interface defects.

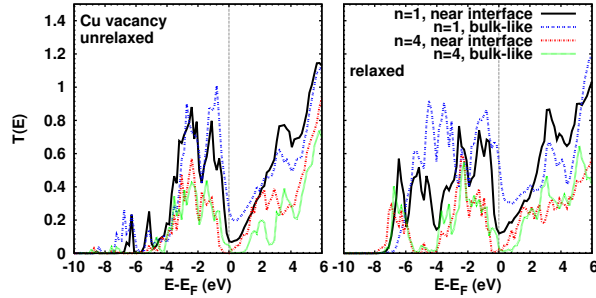


FIG. 5. (Color online) Transmission coefficients for Cu vacancies, before (left) and after (right) structural optimization; compare Fig. 1, (f) and (g). While the overall behavior is similar before and after relaxation, one notes an increase around -7 eV and a decrease for energies far above E_F due to optimization. At E_F , the transmission is higher for $n = 1$ compared to $n = 4$ and for a bulk-like compared to near-interface defects. Slightly above E_F , a Cu bulk vacancy creates for $n = 4$ a strong transport gap, for both the relaxed and unrelaxed situation.

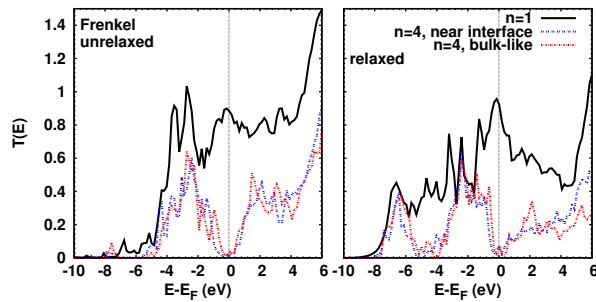


FIG. 6. (Color online) Transmission coefficients for $n = 1$ and 4 heterojunctions with Frenkel defects, before (left) and after (right) structural optimization. The labels “near-interface” and “bulk-like” refer to (h) and (i) in Fig. 1, respectively. For $n = 1$, of course, there is only one type of Frenkel defect. Due to the optimization, there is a drastic change in the transmission in the energy range -6 eV to E_F . A pronounced peak near -7 eV appears for all thicknesses. Again an increase of the transmission at E_F is found for $n = 1$ and 4 due to relaxation, while the transmission above E_F is reduced.

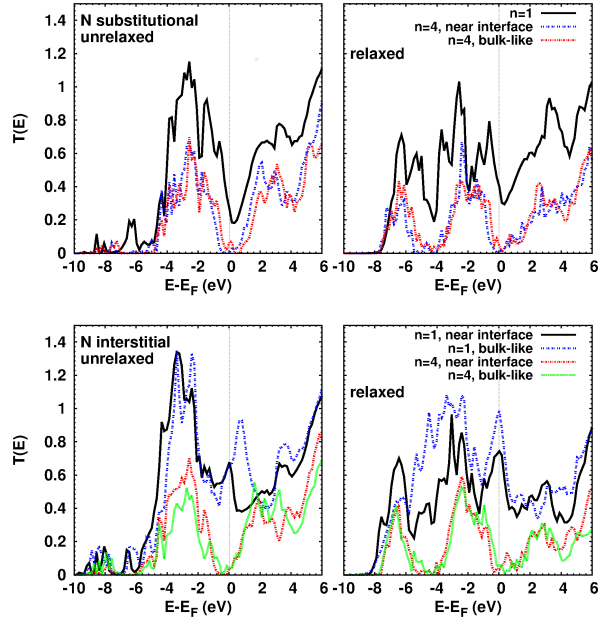


FIG. 7. (Color online) Transmission coefficients for N substitutional (top) and interstitial doping (bottom), before (left) and after (right) structural optimization. For the $n = 1$ heterojunction, besides the appearance of strong transmission around -7 eV as discussed before, the shift of the the extrema near the Fermi energy upon relaxation is remarkable, in particular, for N interstitial doping. The transmission is found to depend significantly on the location of the N interstitial only for the optimized case. For $n = 4$, it appears that transmission is slightly higher after relaxation for bulk-like doping (substitutional or interstitial) compared to near-interface doping.

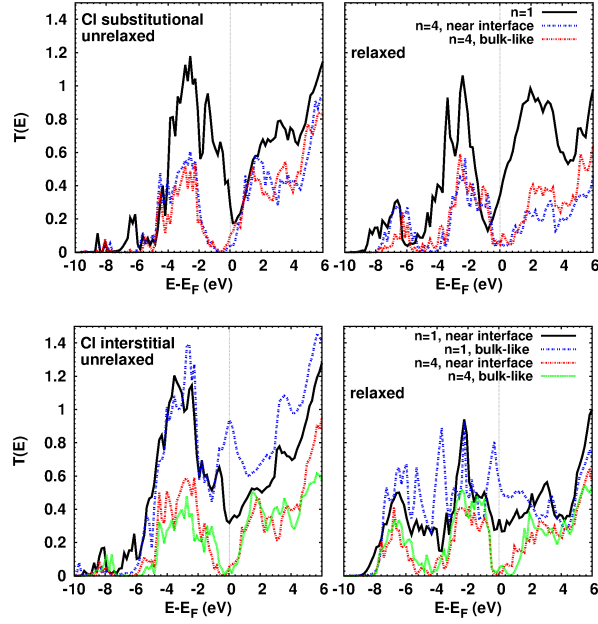


FIG. 8. (Color online) Transmission coefficients for Cl substitutional (top) and interstitial doping (bottom), before (left) and after (right) structural optimization. For substitutional doping, the position of the extrema at E_F for the $n = 1$ unrelaxed system are similar to the N case, compare Fig. 7, whereas the situation is different for $n = 4$. For interstitial doping, on the other hand, for both $n = 1$ and 4 the behavior of the unrelaxed systems is close to the N interstitial. The conductances of the optimized structures are less or equal to the corresponding unoptimized ones for $n = 1$. Again for $n = 4$ the conductances are found to increase upon optimization.

-
- [1] Zakutayev, A., Stevanovic, V. & Lany, S. Non-equilibrium Alloying controls optoelectronic properties in Cu₂O thin films for photovoltaic absorber applications. *Appl. Phys. Lett.* **106**, 123903 (2015).
- [2] Nguyen, S. H., Lim, J.-C. & Lee, J.-K. Improving the performance of silicon anode in lithium-ion batteries by Cu₂O coating layer. *J. Appl. Electrochem.* **44**, 353–360 (2014).
- [3] Deng, S. *et al.* Reduced Graphene oxide conjugated Cu₂O nanowire mesocrystals for high-performance NO₂ gas sensor. *J. Am. Chem. Soc.* **134**, 4905–4917 (2012) .
- [4] Meyer, B. K. *et al.* Binary Copper oxide semiconductors: From materials towards devices. *Phys. Status Solidi B* **249**, 1487–1509 (2012).
- [5] Ruiz, E., Alvarez, S., Alemany, P. & Evarestov, R. A. Electronic Structure and properties of Cu₂O. *Phys. Rev. B* **56**, 7189–7196 (1997).
- [6] Buljan, A., Llundell, M., Ruiz, E. & Alemany, P. Color and conductivity in Cu₂O and CuAlO₂: A theoretical analysis of d¹⁰ . . . d¹⁰ interactions in solid-state compounds. *Chem. Mater.* **13**, 338–344 (2001).
- [7] Heinemann, M., Eifert, B. & Heiliger, C. Band structure and phase stability of the copper oxides Cu₂O, CuO, and Cu₄O₃. *Phys. Rev. B* **87**, 115111 (2013).
- [8] Filippetti, A. & Fiorentini, V. Coexistence of ionic and metallic bonding in noble-metal oxides. *Phys. Rev. B* **72**, 035128 (2005).
- [9] Nolan, M. & Elliott, S. D. The p-Type conduction mechanism in Cu₂O: A first principles study. *Phys. Chem. Chem. Phys.* **8**, 5350–5358 (2006).
- [10] Yoshimura, M., Revcolevschi, A. & Castaing, J. Thermogravimetric study of the non-stoichiometry of cuprite Cu₂O. *J. Mater. Sci.* **11**, 384–386 (1976).
- [11] Xue, J. & Dieckmann, R. The non-stoichiometry and the point defect structure of cuprous oxide (Cu_{2-δ}O). *J. Phys. Chem. Solids* **51**, 1263–1275 (1990).
- [12] Porat, O. & I. Riess, I. Defect chemistry of Cu_{2-y}O at elevated temperatures. part i: Non-stoichiometry, phase width and dominant point defects. *Solid State Ionics* **74**, 229–238 (1994).
- [13] Aggarwal, S., Topfer, J., Tsai, T. L. & Dieckmann, R. Point defects and transport in binary and ternary, non-stoichiometric oxides. *Solid State Ionics* **101**, 321–331 (1997).

- [14] Kim, J. Y., Rodriguez, J. A., Hanson, J. C., Frenkel, A. I. & Lee, P. L. Reduction of CuO and Cu₂O with H₂: H embedding and kinetic effects in the formation of suboxides. *J. Am. Chem. Soc.* **125**, 10684–10692 (2003).
- [15] Isseroff, L. Y. & Carter, E. A. Electronic structure of pure and doped cuprous oxide with copper vacancies: Suppression of trap states. *Chem. Mater.* **25**, 253–265 (2013).
- [16] Musa, A. O., Akomolafe, T. & Carter, M. J. Production of cuprous oxide, a solar cell material, by thermal oxidation and a study of its physical and electrical properties. *Sol. Energy Mater. Sol. Cells* **51**, 305–316 (1998).
- [17] Ishizuka, S., Kato, S., Okamoto, Y. & Akimoto, K. Nitrogen doping into Cu₂O thin films deposited by reactive radio-frequency magnetron sputtering. *Jpn. J. Appl. Phys.* **40**, 2765–2768 (2001).
- [18] Li, J. *et al.* Probing defects in nitrogen-doped Cu₂O. *Sci. Rep.* **4**, 7240 (2014).
- [19] Ishizuka, S., Kato, S., Maruyama, T. & Akimoto, K. Control of hole carrier density of polycrystalline Cu₂O thin films by Si doping. *Appl. Phys. Lett.* **80**, 950–952 (2002).
- [20] Nemoto, T. & Nakano, T. The effect of silicon on cuprous oxide. *Jpn. J. Appl. Phys.* **6**, 543–544 (1967).
- [21] O’Keeffe, M. & Moore, W. J. Electrical conductivity of monocrystalline cuprous oxide. *J. Chem. Phys.* **35**, 1324–1328 (1961).
- [22] Wei, M. *et al.* Room temperature ferromagnetism in bulk Mn-doped Cu₂O. *Appl. Phys. Lett.* **86**, 072514 (2005).
- [23] Kale, S. *et al.* Magnetism in cobalt-doped Cu₂O thin films without and with Al, V, or Zn codopants. *App. Phys. Lett.* **82**, 2100–2102 (2003).
- [24] Kikuchi, N. & Tonooka, K. Electrical and structural properties of Ni-doped Cu₂O films prepared by pulsed laser deposition. *Thin Solid Films* **486**, 33–37 (2005).
- [25] Kikuchi, N., Tonooka, K. & Kusano, E. Mechanisms of carrier generation and transport in Ni-doped Cu₂O. *Vacuum* **80**, 756–760 (2006).
- [26] Tseng, C. C., Hsieh, J. H., Liu, S. J. & Wu, W. Effects of Ag contents and deposition temperatures on the electrical and optical behaviors of Ag-doped Cu₂O thin films. *Thin Solid Films* **518**, 1407–1410 (2009).
- [27] Papadimitriou, L., Dimitriadis, C. A., Dozsa, L. & Andor, L. Acceptor states distributed in energy in Cd-doped Cu₂O. *Solid State Commun.* **71**, 181–185 (1989).

- [28] Papadimitriou, L. DLTS evaluation of nonexponential transients of defect levels in cuprous oxide (Cu_2O). *Solid-State Electron.* **36**, 431–434 (1993).
- [29] Soon, A., Cui, X. Y., Delley, B., Wei, S. H. & Stampfl, C. Native defect-induced multifarious magnetism in nonstoichiometric cuprous oxide: First-principles study of bulk and surface properties of $\text{Cu}_{2-\delta}\text{O}$. *Phys. Rev. B* **79**, 035205 (2009).
- [30] Sieberer, M., Redinger, J. & Mohn, P. Electronic and magnetic structure of cuprous oxide Cu_2O doped with Mn, Fe, Co, and Ni: A density-functional theory study. *Phys. Rev. B* **75**, 035203 (2007).
- [31] Martinez-Ruiz, A., Moreno, M. G. & Takeuchi, N. First principles calculations of the electronic properties of bulk Cu_2O , clean and doped with Ag, Ni, and Zn. *Solid State Sci.* **5**, 291–295 (2003).
- [32] Liu, D., Zhu, Y. F. & Jiang, Q. DFT study of CO oxidation on Cu_2O -Au interfaces at Au-Cu alloy surfaces. *RSC Adv.* **5**, 1587–1597 (2015).
- [33] Zhang, L., Kim, H. Y. & Henkelman, G. CO oxidation at the Au-Cu interface of bimetallic nanoclusters supported on $\text{CeO}_2(111)$. *J. Phys. Chem. Lett.* **4**, 2943–2947 (2013).
- [34] Blajiev, O. L. & Hubin, A. The effect of silicon on cuprous oxide. *Electrochim. Acta* **50**, 4297–4307 (2005).
- [35] Jayakrishnan, R. Photovoltaic response of $\text{Cu}_2\text{O}/\text{In}_2\text{S}_3$ hetero-structure grown on Cu substrate. *Mater. Sci. Semicond. Process.* **16**, 1608–1612 (2013).
- [36] Yang, M., Zhu, L., Li, Y., Cao, L. & Guo, Y. Asymmetric interface band alignments of $\text{Cu}_2\text{O}/\text{ZnO}$ and $\text{ZnO}/\text{Cu}_2\text{O}$ heterojunctions. *J. Alloys Comp.* **578**, 143–147 (2013).
- [37] De Los Santos Valladares L. *et al.* Crystallization and electrical resistivity of Cu_2O and CuO obtained by thermal oxidation of Cu thin films on SiO_2/Si substrates. *Thin Solid Films* **520**, 6368–6374 (2012).
- [38] Jayathilaka, K. M. D. C., Kapaklis, V., Siripala, W. & Jayanetti, J. K. D. S. Surface treatment of electrodeposited n-type Cu_2O thin films for applications in Cu_2O based devices. *Phys. Status Solidi RRL* **8**, 592–595 (2014).
- [39] Soler, J. M. *et al.* Ab initio derivation of the electronic structure properties across the Cu- Cu_2O interface. *J. Phys.: Condens. Matter* **14**, 2745–2779 (2002).
- [40] Rocha, A. R. *et al.* Towards molecular spintronics. *Nature Mater.* **4**, 335–339 (2005).

- [41] Rocha, A. R. *et al.* Spin and molecular electronics in atomically generated orbital landscapes. *Phys. Rev. B* **73**, 085414 (2006).
- [42] Rungger, I. & Sanvito, S. Algorithm for the construction of self-energies for electronic transport calculations based on singularity elimination and singular value decomposition. *Phys. Rev. B* **78**, 035407 (2008).
- [43] Perdew, J. P., Burke, K. & Ernzerhof, M. Generalized gradient approximation made simple. *Phys. Rev. Lett.* **77**, 3865–3868 (1996).
- [44] Kleinman, L. & Bylander, D. M. Efficacious form for model pseudopotentials. *Phys. Rev. Lett.* **48**, 1425–1428 (1982).
- [45] Louie, S. G., Froyen, S. & Cohen, M. L. Nonlinear ionic pseudopotentials in spin-density-functional calculations. *Phys. Rev. B* **26**, 1738–1742 (1982).
- [46] Boys, S. F. & Bernardi, F. The calculation of small molecular interactions by the differences of separate total energies. Some procedures with reduced errors. *Mol. Phys.* **19**, 553 (1970).
- [47] Raebiger, H., Lany, S. & Zunger, A. Origins of the p-type nature and cation deficiency in Cu_2O and related materials. *Phys. Rev. B* **76**, 045209 (2007).
- [48] Scanlon, D. O., Morgan, B. J. & Watson, G. W. Modeling the polaronic nature of p-type defects in Cu_2O : The failure of GGA and GGA+U. *J. Chem. Phys.* **131**, 124703 (2009).
- [49] Scanlon, D. O., Morgan, B. J., Watson, G. W. & Walsh, A. Acceptor levels in p-type Cu_2O : Rationalizing theory and experiment. *Phys. Rev. Lett.* **103**, 096405 (2009).
- [50] De Jongh, P. E., Vanmaekelbergh, D. & Kelly, J. J. Photoelectrochemistry of electrodeposited Cu_2O . *J. Electrochem. Soc.* **147**, 486–489 (2000).
- [51] Garuthara, R. & Siripala, W. Photoluminescence characterization of polycrystalline n-type Cu_2O films. *J. Lumin.* **121**, 173–178 (2006).
- [52] Zouaghi, M., Tapiero, M., Zielinger, J. P. & Burgraf, R. Hall mobility and hole density in photoactivated Cu_2O single crystals. *Solid State Commun.* **8**, 1823–1825 (1970).
- [53] Fujinaka, M. & Berezin, A. A. Cuprous oxide-indium-tin oxide thin film photovoltaic cells. *J. Appl. Phys.* **54**, 3582–3588 (1983).
- [54] Autes, G., Barreteau, C., Spanjaard, D. & Desjonqueres, M.-J. Electronic transport in iron atomic contacts: From the infinite wire to realistic geometries. *Phys. Rev. B* **77**, 155437 (2008).